

Combustion Simulation with Lattice Boltzmann Method in a Three-Dimensional Porous Structure

by

Kazuhiro YAMAMOTO

Department of Mechanical Engineering, Nagoya University

Furo-cho, Chikusa-ku, Nagoya, Aichi 464-8603, JAPAN

Naoki TAKADA and Masaki MISAWA

National Institute of Advanced Industrial Science and Technology

16-1 Onogawa, Tsukuba, Ibaraki 305-8569, JAPAN

Correspondence: Kazuhiro YAMAMOTO
Department of Mechanical Engineering
Faculty of Engineering
Nagoya University
Furo-cho, Chikusa-ku, Nagoya, Aichi 464-8603, JAPAN
Tel: +81-52-789-4471, Fax: +81-52-789-4471
E-mail: kazuhiro@mech.nagoya-u.ac.jp

Paper ID: PID28912

Short Running Title: Combustion Simulation in 3D Porous Structure

Keywords: Lattice Boltzmann Method, 3D Computer Tomography, Porous Media,
Diesel Particulate Filter, Soot

Combustion Simulation with Lattice Boltzmann Method in a Three-Dimensional Porous Structure

by

K. YAMAMOTO¹, N. TAKADA², and M. MISAWA²

¹Department of Mechanical Engineering, Nagoya University

Furo-cho, Chikusa-ku, Nagoya, Aichi 464-8603, JAPAN

²National Institute of Advanced Industrial Science and Technology

16-1 Onogawa, Tsukuba, Ibaraki 305-8569, JAPAN

(Abstract)

To simulate the flow in three-dimensional porous structure, we have used the Lattice Boltzmann method (LBM). The distribution function for flow, temperature, and concentration fields are solved to simulate the regeneration process of diesel particulate filter (DPF). For a benchmark study, we have conducted the calculation in simple geometry. To change the flow characteristics such as porosity and tortuosity, the obstacles of different number and size are selected, which are randomly placed in the duct. The flow pattern is changed with obstacle size even at the same porosity. To confirm the validity of our calculation, the results are compared with the empirical relationships of the Blake-Kozeny and Ergun equations, in the non-dimensional form using the Ergun coordinates of Reynolds number and friction factor. Numerical results show good agreements with the Blake-Kozeny equation, although the friction factor with larger obstacle size is higher than the empirical predictions. The soot combustion is well simulated to show the effects of oxygen on the reaction rate. Finally, the real porous geometry has been tested. The porous structure of Ni-Cr metal has been obtained by three-dimensional computer tomography technique. Results show that, the inhomogeneous flow is observed and there are regions where the temperature is locally higher. This information is indispensable for the better design of DPF. LBM can be a good tool for combustion simulation in porous media.

1. Introduction

Although diesel engines have an advantage of low fuel consumption in comparison with gasoline engines, several problems must be solved. One of the major concerns is that diesel exhaust gas has more particle matters (PM) including soot, which are suspected to be linked to human carcinogen. For this reason, more strict exhaust emissions standards such as Euro V in 2008 will be set in many countries. In Japan, the Tokyo municipal government has begun to regulate diesel-powered commercial vehicles that fail to meet the new emission standards.

As one of the key technologies, a diesel particle filter (DPF) has been developed to reduce particle matters (PM) in the after-treatment of exhaust gas. Some products have been introduced at the Frankfurt Motor Show in 2003. This can be applied to satisfy more strict regulations for diesel emissions, coupled with improvements of combustion conditions. In simple explanation of DPF, it traps the particles when exhaust gas passes its porous structure. Since the filter wall would readily be plugged with particles in a short time, the accumulated particles must be removed. Usually, the filter is heated to burn the particles in combustion. It is called filter regeneration process. However, it is expected that the outer heating with the particle burning may destroy the porous structure. Then, the thermal durable filter is plausible to maintain the low level of emissions in the long term [1]. So far, the filter has been developed mainly by experiments, and there may not be enough information to observe and understand the phenomena in DPF. For better design of the DPF with efficiency and durability, it is necessary to conduct simulation with combustion in porous media. However, in conventional computational code, it is very challenging to deal with this process, because we need to consider the complex geometry with chemical reaction.

Recently, the Lattice Boltzmann method (LBM) has been proposed into an alternative and promising numerical scheme for simulating fluid flows [2]. Main advantages of LBM are the simplicity of the algorithm and the flexibility for complex geometries. It has been widely applied for the flow in porous media [3-9].

Therefore, if the combustion reaction is included in this numerical method, it is possible to investigate directly the local heat and mass transfer in DPF, which is normally impossible to obtain by measurements.

In the present study, the flow in three-dimensional porous structure is simulated by LBM. For a benchmark study, we conduct the calculation in simple geometry. The obstacles are randomly inserted in the duct to simplify the complex geometry of porous media. The number and size of the obstacle are selected to change the flow characteristics such as porosity. In addition, we use the real porous material in the simulation. Three-dimensional computer tomography technique (3D CT) is applied to obtain inner structure of a Ni-Cr metal [10,11]. The combustion reaction is included for the simulation of regeneration process of DPF, using both geometries.

2. Numerical Method

The fundamental idea of the LBM is to construct simplified kinetic models that incorporate the essential physics of microscopic or mesoscopic processes so that the macroscopic averaged properties obey the desired macroscopic equations such as the N-S equation. The kinetic equation provides any of the advantages of molecular dynamics, including clear physical pictures, easy implementation of boundary conditions, and fully parallel algorithms [2]. The LBM fulfills these requirements in a straightforward manner.

So far, many benchmark studies have been conducted. For example, He and Doolen have simulated the flow around two-dimensional circular cylinder to show the time evolution of vortex shedding [12]. Martinez et al. have examined the turbulence in shear layer, and the turbulent flow can be well simulated at a relatively high Reynolds number of 10,000 [13]. Also, simulations of multiphase flow have been conducted [14]. The special treatment is not needed and each phase such as gas and liquid phases can be treated equally.

As for the combustion simulation, we have tested several flow geometries using LBM. For example,

the counter-flow premixed flames have been simulated [15]. This is the first LB simulation on combustion, although coupled approach has been conducted to simulate flow field by LBM and temperature and concentration fields by a finite difference scheme [16]. To validate the LB simulation, we have compared our results with those by conventional method, solving differential conservation equations of mass, momentum, energy, and species. It has been demonstrated that the counter-flow flame structure is well simulated, where both results are perfectly matched. In addition, the turbulent flame has been simulated using the conserved scholar approach [17]. The detailed chemistry and three-dimensional scheme have been also tested in our recent study [18]. It has been concluded that LBM can be used for combustion simulation.

Here, we explain the numerical procedure [15]. The flow is described by the lattice BGK equation in terms of the distribution function. The 3D LBGK model (D3Q15 model) [6] evolves on the lattice space with the following 15 discrete velocities in Fig. 1.

$$\begin{aligned}
 & [c_1 \quad c_2 \quad c_3 \quad c_4 \quad c_5 \quad c_6 \quad c_7 \quad c_8 \quad c_9 \quad c_{10} \quad c_{11} \quad c_{12} \quad c_{13} \quad c_{14} \quad c_{15}] \\
 & = c \begin{bmatrix} 1 & -1 & 0 & 0 & 0 & 0 & 1 & -1 & 1 & -1 & 1 & -1 & 1 & -1 & 0 \\ 0 & 0 & 1 & -1 & 0 & 0 & 1 & -1 & 1 & -1 & -1 & 1 & -1 & 1 & 0 \\ 0 & 0 & 0 & 0 & 1 & -1 & 1 & -1 & -1 & 1 & 1 & -1 & -1 & 1 & 0 \end{bmatrix} \quad (1)
 \end{aligned}$$

where c is the advection speed. The evolution equation using the pressure distribution function is,

$$p_\alpha(\mathbf{x} + \mathbf{c}_\alpha \delta_t, t + \delta_t) - p_\alpha(\mathbf{x}, t) = -\frac{1}{\tau} [p_\alpha(\mathbf{x}, t) - p_\alpha^{eq}(\mathbf{x}, t)] \quad (2)$$

where δ is the time step, and τ is the relaxation time that controls the rate of approach to equilibrium. The equilibrium distribution function, p_α^{eq} , is given by

$$p_\alpha^{eq} = w_\alpha \left\{ p + p_0 \left[3 \frac{(\mathbf{c}_\alpha \cdot \mathbf{u})}{c^2} + \frac{9}{2} \frac{(\mathbf{c}_\alpha \cdot \mathbf{u})^2}{c^4} - \frac{3}{2} \frac{\mathbf{u} \cdot \mathbf{u}}{c^2} \right] \right\} \quad (3)$$

where $w_\alpha = 1/9$ ($\alpha = 1$ to 6), $w_\alpha = 1/72$ ($\alpha = 7$ to 14), and $w_{15} = 2/9$. The sound speed, c_s , is $c/\sqrt{3}$ with $p_0 = \rho_0 RT_0 = \rho_0 c_s^2$. Here, p_0 and ρ_0 are the pressure and density at the room temperature. In this study, to consider the variable density, we adopt the low Mach number approximation [16]. The pressure and local velocity of $\mathbf{u} = (u_x, u_y, u_z)$ are obtained using the ideal gas equation.

$$p = \sum_{\alpha} p_\alpha \quad (4)$$

$$\mathbf{u} = \frac{\rho_0}{\rho} \frac{1}{p_0} \sum_{\alpha} \mathbf{c}_\alpha p_\alpha \quad (5)$$

The relaxation time is related with transport coefficients, such as kinetic viscosity and diffusion coefficient using $\nu = (2\tau - 1)/6 c^2 \delta_t$. Through the Chapman-Enskog procedure, the Navier-Stokes equations are derived from these equations [2]. The LBM formula for temperature and concentration fields is,

$$F_{s,\alpha}(\mathbf{x} + \mathbf{c}_\alpha \delta_t, t + \delta_t) - F_{s,\alpha}(\mathbf{x}, t) = -\frac{1}{\tau_s} [F_{s,\alpha}(\mathbf{x}, t) - F_{s,\alpha}^{eq}(\mathbf{x}, t)] + w_\alpha Q_s, \quad s = T, Y_i \quad (6)$$

where Q_s is the source term due to chemical reaction. The temperature, T , and mass fraction of species, Y_i , are determined by these distribution functions.

$$T = \sum_{\alpha} F_{T,\alpha} \quad (7)$$

$$Y_i = \sum_{\alpha} F_{Y_i, \alpha} \quad (8)$$

For the benchmark study on porous media flow, we test simple geometry to use obstacles with cubic shape in the 3-D duct flow. Figure 2 shows the coordinate and boundary conditions. The calculation domain is $5 \text{ cm} \times 1 \text{ cm} \times 1 \text{ cm}$, and the inflow velocity is 20 cm/s . The total number of grids is $201 (N_x) \times 41 (N_y) \times 41 (N_z)$, with grid size of 0.25 mm . To change the flow characteristics such as porosity and tortuosity, the different number and size of obstacle are used, which are placed randomly in the center part between two dotted lines in this figure. As for the boundary condition, the inflow boundary is adopted at the inlet [19]. The temperature and mass fractions are those of the air at room temperature. At the sidewall, the slip boundary conditions are adopted, considering the symmetry [7]. At the outlet, the pressure is constant, and the gradient of scalar such as temperature and mass fraction is set to be zero. On the surface of the obstacle, the non-slip boundary condition is adopted.

The real geometry is also tested. The porous Ni-Cr metal is used in this calculation. By using a 3D computer tomography (CT) technique [11], we obtain the inner geometry of porous structure. Figure 3 shows this procedure. The material with a height of 5.5 mm and a diameter of 8 mm is scanned. The estimated porosity is 0.57 . We obtain 400 CT images with resolution of $13.75 \mu\text{m/pix}$. The black region is inner space and the white region is the metal. Based on the tomography data, we construct the geometry digitized for 3D calculation.

The combustion simulation is conducted for these two geometries. It is assumed that the soot is homogeneously attached to the porous wall surface. The over-all reaction by Lee et al. is adopted for soot oxidation [20]. For simplicity, any catalytic effects are not considered. The oxygen concentration in inflow is changed. It can be an important parameter in engine operation, because it is easy to control the oxygen concentration by using the exhaust gas recirculation (EGR) [21], in order to prevent an abrupt temperature rise

from damaging the local structure of DPF.

3. Results and Discussion

3.1 Flow in Simple Geometry

Figure 4 shows the distribution of non-dimensional velocity in the x-direction, u_x/U_{in} . The obstacle size is of $D = 2, 3, 6$ in lattice space, which are 0.5, 0.75, and 1.5 mm in real scale. The porosity, e , is set to be 0.9 for three cases. The profiles in x - y and x - z planes are shown, which are the cross section at the center axis. It is found that the flow is largely fluctuated in the area with obstacles and the flow direction is changed, even when the flow is uniform at the inlet. The velocity is locally accelerated in the narrow path, since the obstacle is randomly placed. As a whole, the flow is smooth when the obstacle size is small ($D = 2$). In the case of $D = 6$, the negative velocity is observed, which means that the recirculation flow exists. Therefore, with different size of obstacle, the flow pattern is changed at the same porosity.

Next, the pressure distribution is examined for the above three cases, which is an important parameter in porous media flow. Figure 5 shows the pressure distribution, which is the mean value in the y - z plane, normalized by the constant pressure at the outlet. In the area with obstacles, the pressure starts to decrease almost linearly, although it slightly fluctuates for $D = 3$ and 6. After passing this region, the pressure is almost constant. To compare three cases, it is found that, as the obstacle size is smaller with the porosity constant, the pressure at the inlet is larger. It could be explained by the fact that the surface of the obstacle is larger with smaller obstacle, causing the larger effect of shear forces.

In the theory for the transport in porous media [22], it is assumed that its inner structure is modeled as a bundle of capillary tubes. Only shear forces in a laminar Poiseuille like flow are taken into account. Then, the pressure drop is related with a bed friction factor. The higher friction coefficient is considered to include the

tortuosity. Comparing the theoretical formula with experimental results, the empirical relationships of the Blake-Kozeny equation and the Ergun equation are derived, which are usually used for flow at low and high Reynolds numbers, respectively. Then, we compare our results with these empirical equations to validate our calculation.

First, the hydraulic radius, R_h , and the equivalent diameter of the obstacles, D_p must be determined.

$$R_h = \frac{\text{volume available for flow}}{\text{total wetted surface}} \quad (9)$$

$$D_p = 6R_h \frac{1-e}{e} \quad (10)$$

The derivation has been explained in Ref. 22. Introducing the following friction factor, f , and Reynolds number, Re , defined by

$$f = \left(-\frac{dp}{dx} \right) \frac{D_p}{\rho_0 U_{in}^2} \frac{e^3}{(1-e)} \quad (11)$$

$$Re = \frac{U_{in} D_p}{\nu(1-e)} \quad (12)$$

the Blake-Kozeny equation and the Ergun equation are as follows:

$$f = 150 / Re \quad (13)$$

$$f = 150 / Re + 1.75 \quad (14)$$

Usually, f and Re are called Ergun coordinates, and these two empirical equations show good prediction for the experimental data.

The numerical results at $e = 0.8$ and 0.9 and empirical equations are shown in Fig. 6, plotting the values under quasi-steady state where the velocity and pressure have only small perturbation. The pressure gradient appearing in Eq. (11) is estimated by the least squares method. Here, by changing the inflow velocity in the range of 10 to 20 cm/s, we obtain several data. In the case of $D = 2$ and $e = 0.9$, we monitor f and Re until steady state is achieved to observe the flow evolution. The numerical results including the unsteady case show good agreements with the Blake-Kozeny equation, although the friction factor is relatively higher with $D = 5$, 6.

It should be noted that the flow is relatively stable when the obstacle size is small. However, if its size is large enough, there appear the vortices behind the obstacle, which is observed by Inamuro et al. [7]. They have pointed out that the numerical data for flow with vortices approaches to the Ergun equation, which is valid for turbulent flow. Then, our results are reasonable, and it is possible to simulate the flow in porous media by considering this simple flow geometry with obstacles.

Next, the combustion flow is simulated. It is assumed that the soot is homogeneously attached to the wall surface with soot mass fraction of 0.1. When the wall temperature is raised, the soot is burned to react with oxygen in the air. Time, t , is counted after we set the wall temperature (1200 K). Figure 7 shows the distributions in the x - y plane for temperature of T , mass fraction of oxygen and soot of Y_{O_2} and Y_C , and the reaction rate of W_C . The porosity is 0.9 and the obstacle size is of $D = 3$ and $t = 0.63$ s. It is found that the oxygen concentration around the wall is decreased by the reaction with soot. Then, the maximum temperature is higher than the wall temperature. It is interesting to note that the reaction rate locally varies, simply because the flow is different due to the random placement of obstacles.

In addition, we change the oxygen concentration in inflow, which is an important parameter to control the reaction rate. Here, nitrogen is added in the air. We set the oxygen concentration (mass fraction) to be 0.233 (air) and 0.1. As seen in Fig.7(d), the reaction rate is locally changed. To make clear the effect of oxygen

concentration, the reaction rate averaged at the wall surface of all obstacles is calculated. Results are shown in Fig. 8. As the oxygen concentration is higher, the mean reaction rate is increased. That is, the reaction of soot will be completed at the earlier stage, compared with dilution case. This is very reasonable, and the capability of combustion simulation in porous media is demonstrated.

3.2 Flow in Porous Ni-Cr Metal

Finally, we simulate combustion field using the real geometry of Ni-Cr metal. Figure 9(a) shows the porous structure and calculation domain. The same grid number of $201 (N_x) \times 41 (N_y) \times 41 (N_z)$ is used. Porous wall geometry is extracted from the CT data in Fig. 3, inserted to $X = 50$ to 150 , where X is the lattice coordinate in LBM. Total size is $2.75 \text{ mm } (x) \times 0.55 \text{ mm } (y) \times 0.55 \text{ mm } (z)$. The inlet velocity, U_{in} , is 20 m/s , and the soot concentration at the wall is $Y_c = 0.1$. The wall temperature is 1200 K . Figure 9(b) shows the non-dimensional velocity in the x -direction, $VX_I (= u_x/U_{in})$. The velocity vector is also shown. The local velocity varies largely inside the porous media. The maximum velocity is about 8 times larger than the inflow velocity due to the heat expansion.

To examine the combustion field in detail, we obtain the profiles at the cross section. Figure 10 shows the distributions of porous wall, velocity in the x -direction, temperature, and mass fraction of oxygen. These are profiles in x - y and y - z planes. The positions to obtain these cross sections are shown by dotted line in Fig. 10(a). It is clearly found that the velocity is accelerated in the region where the path is narrowed. The temperature is increased by soot combustion near the wall surface, and the local temperature is different due to the inhomogeneous porous structure. This local information is indispensable to improve the thermal duration of DPF. It is demonstrated that the combustion is well simulated in porous media using LBM.

4. Conclusions

To simulate the flow in three-dimensional porous structure, we have used the Lattice Boltzmann method (LBM). The distribution function for flow, temperature, and concentration fields are solved to simulate the regeneration process of diesel particulate filter (DPF). For a benchmark study, we have conducted the calculation in simple geometry. To change the flow characteristics such as porosity and tortuosity, the obstacles of different number and size are selected, which are randomly placed in the duct.

The flow pattern is changed with obstacle size even at the same porosity. To confirm the validity of our calculation, the results are compared with the empirical relationships of the Blake-Kozeny and Ergun equations, in the non-dimensional form using the Ergun coordinates of Reynolds number and friction factor. Numerical results show good agreements with the Blake-Kozeny equation, although the friction factor with larger obstacle size is higher than the empirical predictions. The soot combustion is well simulated to show the effects of oxygen on the reaction rate.

Finally, the real porous geometry has been tested. The porous structure of Ni-Cr metal has been obtained by three-dimensional computer tomography technique. Results show that, the inhomogeneous flow is observed and there are regions where the temperature is locally higher. This information is indispensable for the better design of DPF. LBM can be a good tool for combustion simulation in porous media.

Acknowledgements

This work was supported by Japan Society for the Promotion of Science under Grant-in-Aid for Scientific Research (No.15760131).

References

[1] R. A. Searles, D. Bosteels, C. H. Such, A. J. Nicol, J. D. andersson, and C. A. Jemma, F02E310:1-17,

FISITA 2002 World Congress.

- [2] S. Chen, and G D. Doolen, *Annual Reviews of Fluid Mech. Vol.30*, (1998) 329-364.
- [3] G. McNamara and G. Zanetti, *Phys. Rev. Lett.*, **61**, (1988) 2332–2335.
- [4] S. Succi, E. Foti and F. Higuera, *Europhys. Lett.*, **10**, (1989) 433–438.
- [5] A. Cancelliere, C. Chang, E. Foti, D.H. Rothman and S. Succi, *Phys. Fluids A*, **2**, (1990) 2085–2088.
- [6] Y.H. Qian, D. d’Humières and P. Lallemand, *Europhys. Lett.*, **17**, (1992) 479–484.
- [7] T. Inamuro, M. Yoshino, and F. Ogino, *Int. J. Numerical Methods in Fluids* 29 (1999) 737-748.
- [8] J. Bernsdorf, G. Brenner, and F. Durst, *Computer Physics Communications* 129 (2000) 247-255.
- [9] G Brenner, T. Zeiser, T. Weber, and F. Durst, *First Int. Conf. on Applications of Porous Media* (2002) 675-690.
- [10] A. H. Benouali, L. Froyen, M. Wevers, *X-ray Tomography in Material Science*, (2000) 129-153.
- [11] M. Misawa, N. Takada, I. Tiseanu, R. Hirashima, and K. Koizumi, *The Papers of Technical Meeting on Nuclear Energy, IEE Japan*, NE-02-14 (2002) 17-22.
- [12] X. He and G D. Doolen, *Physical Review E* 56-1 (1997) 434-440.
- [13] D. O. Martinez, W. H. Matthaeus, S. Chen, and D. C. Montgomery, *Phys. Fluids* 6 (1994) 1285-1298.
- [14] X. He, Y. Shan, and G D. Doolen, *Phys. Rev. E* 57 (1998) R13-R16.
- [15] K. Yamamoto, X. He, and G D. Doolen, *J. Statistical Physics*, Vol. 7, Nos.1/2 (2002) 367-383.
- [16] O. Filippova and D. Hanel, *J. Comput. Physics*, 158, (2000) 139-160.
- [17] K. Yamamoto, *Int. J. Modern Phys. B*, Nos. 1&2, (2003) 197-200.
- [18] K. Yamamoto, X. He, and G D. Doolen, *JSME Int. J.*, B03-4108, (2004).
- [19] Q. Zou and X. He, *Phys. Fluids* 9 (6) (1997) 1591-1598.
- [20] K. B. Lee, M. W. Thring, and J. M. Beer, *Comb. Flame* 6 (1962) 137-145.
- [21] K. N. Pattas, A. M. Stamataelos, K. N. Kougiannos, G. C. Koltsakis, and P. K. Pistikopoulos, *SAE Paper*

No. 950366 (1996).

[22] R.B. Bird, W.E. Stewart and E.N. Lightfoot, *Transport Phenomena*, Wiley, New York, 1960.

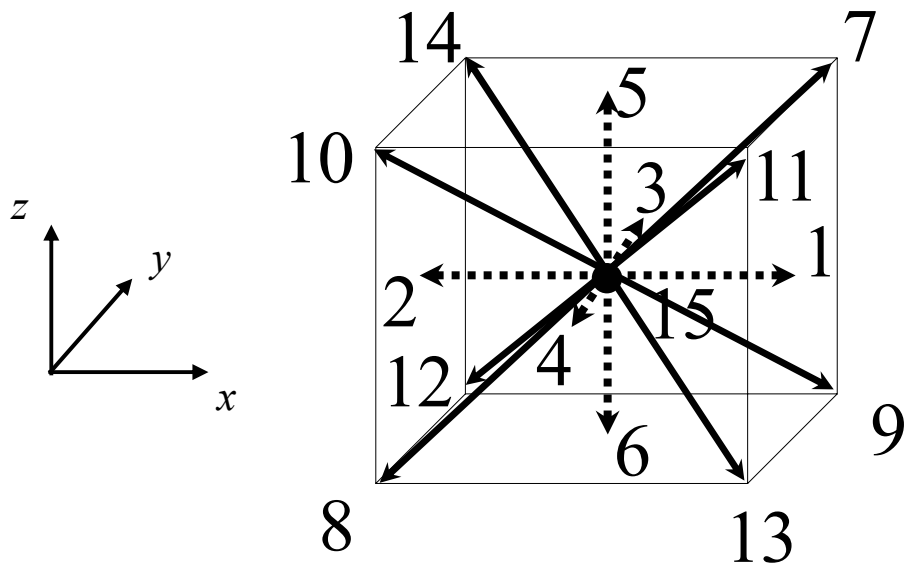


Figure 1 D3Q15 model for 3D simulation.

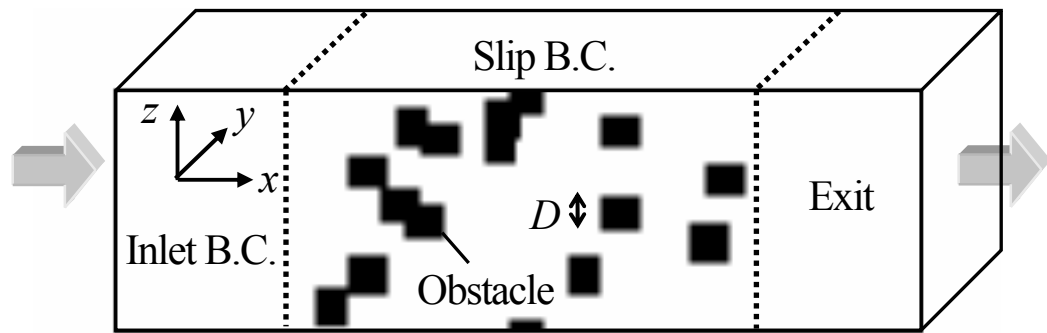


Figure 2 Coordinate and boundary conditions.

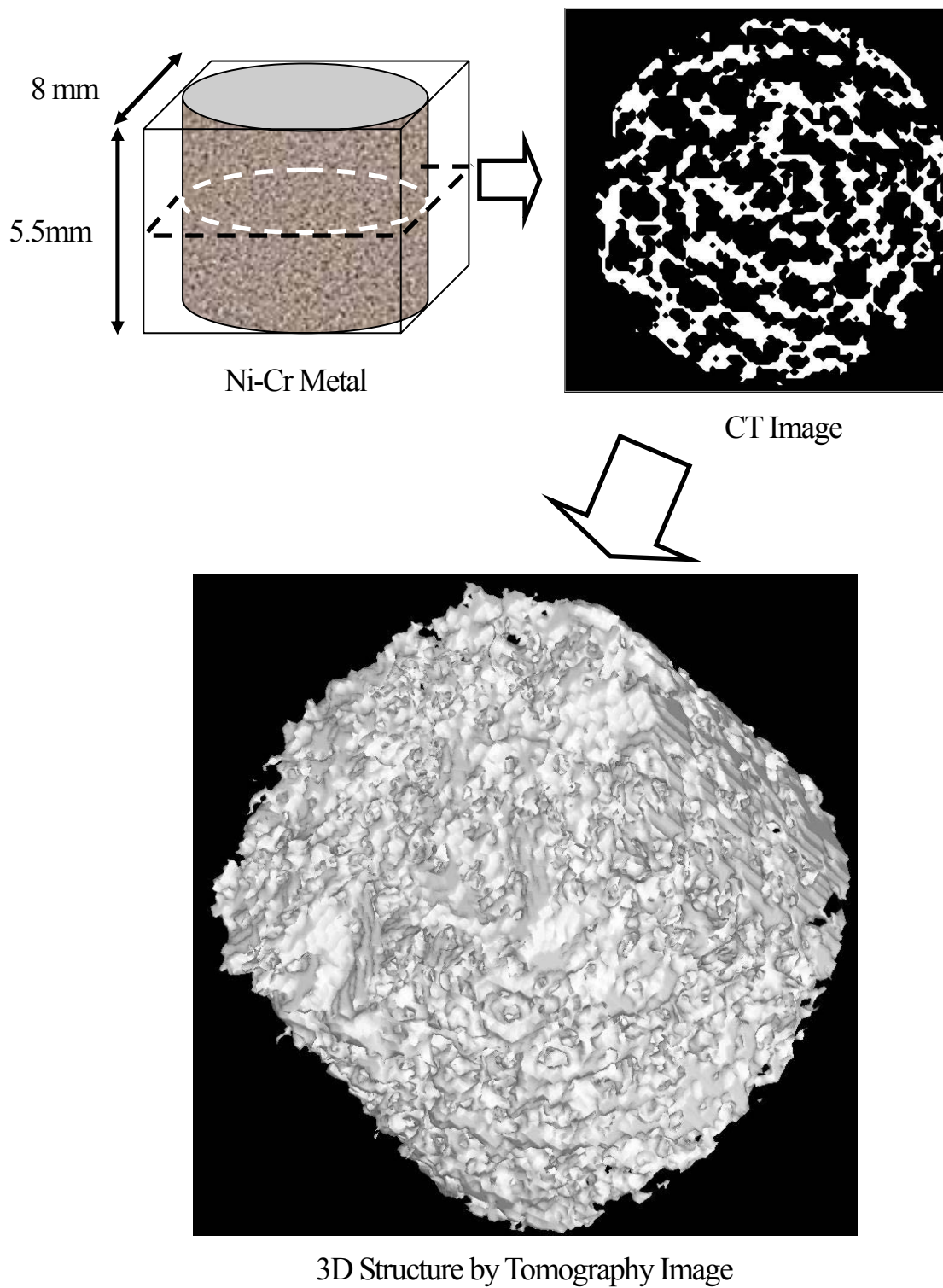


Figure 3 Porous structure of Ni-Cr metal obtained by 3D CT technique with resolution of $13.75 \mu\text{m}/\text{pix}$.

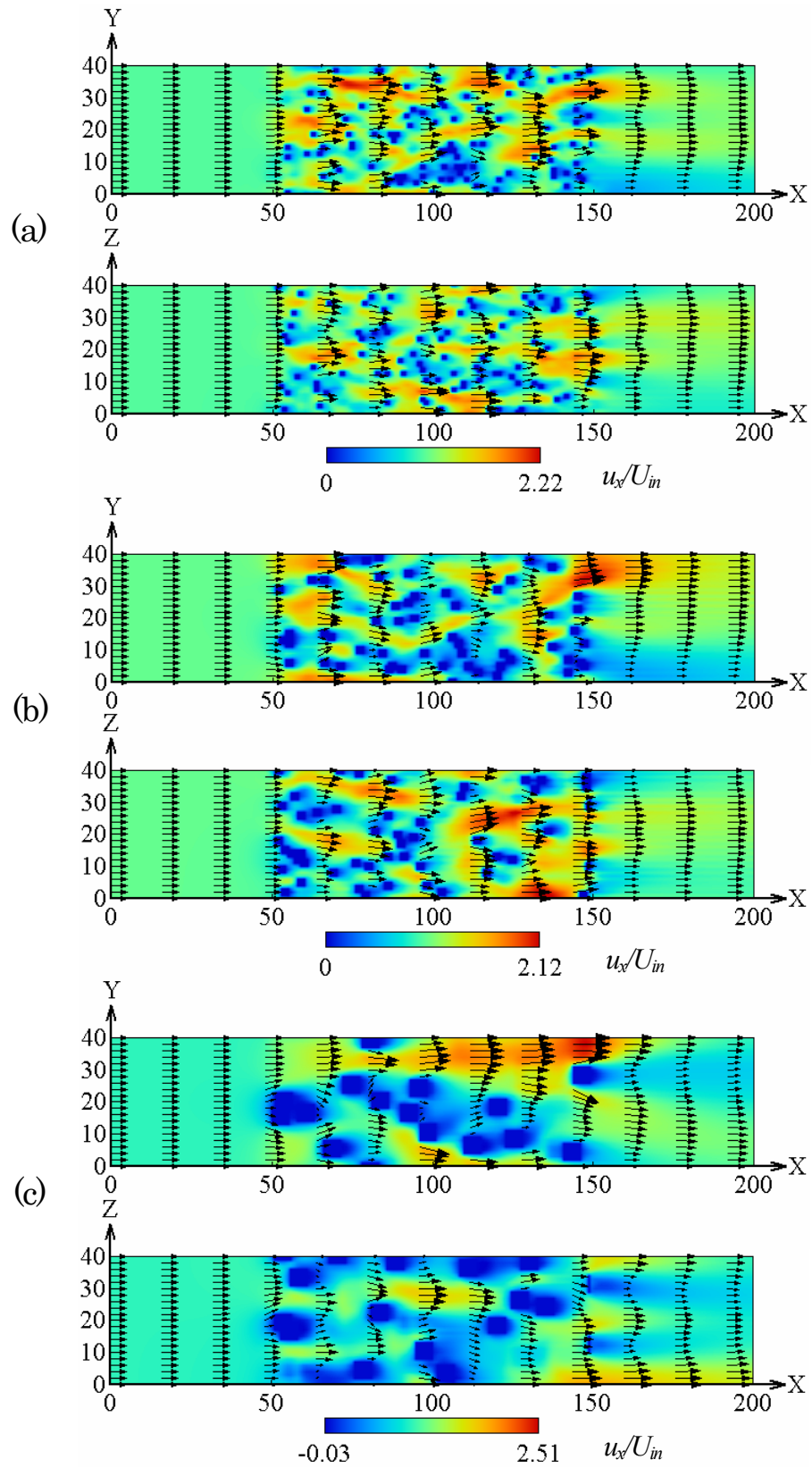


Figure 4 Flow field with obstacles at porosity of $e = 0.9$; (a) $D = 2$, (b) $D = 3$, (c) $D = 6$.

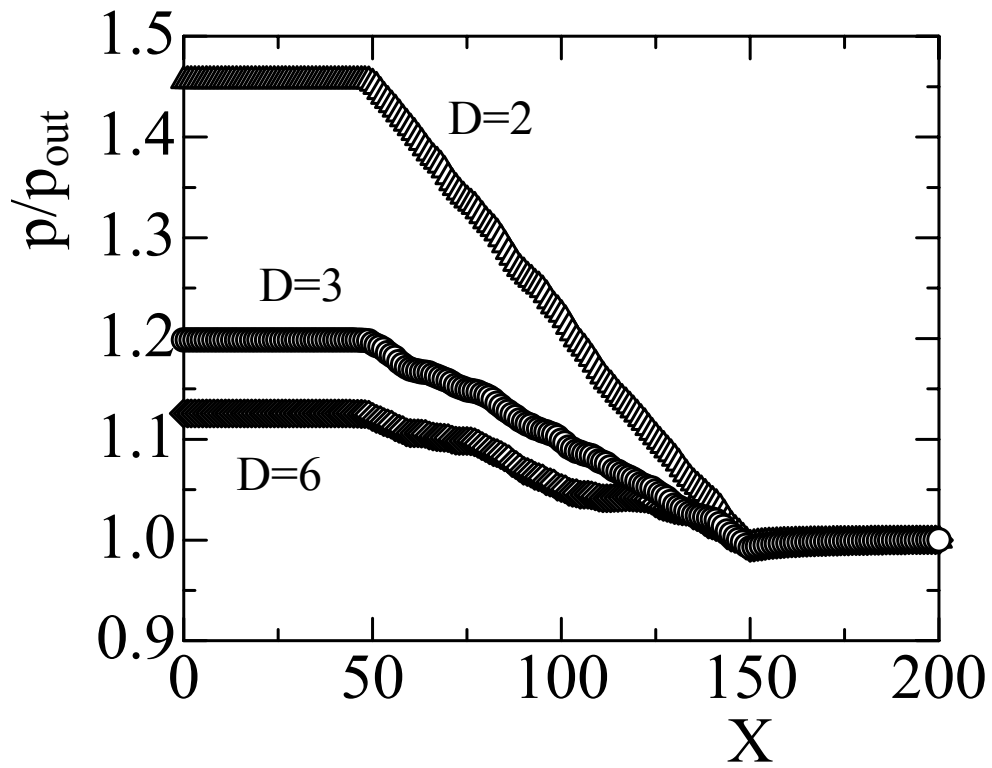


Figure 5 Pressure distribution for $e = 0.9$, $D = 2, 3, 6$.

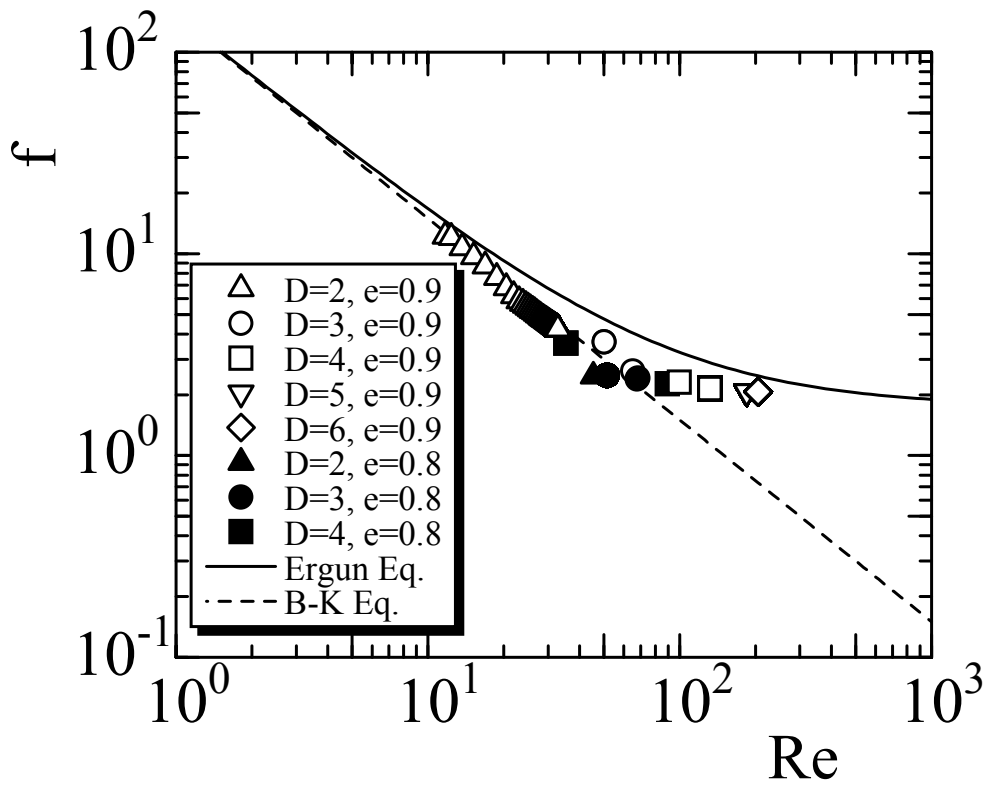


Figure 6 Variations of friction factor with Reynolds number, comparing with empirical relationship of the Ergun equation (solid line) and the Blake-Kozeny equation (dashed line).

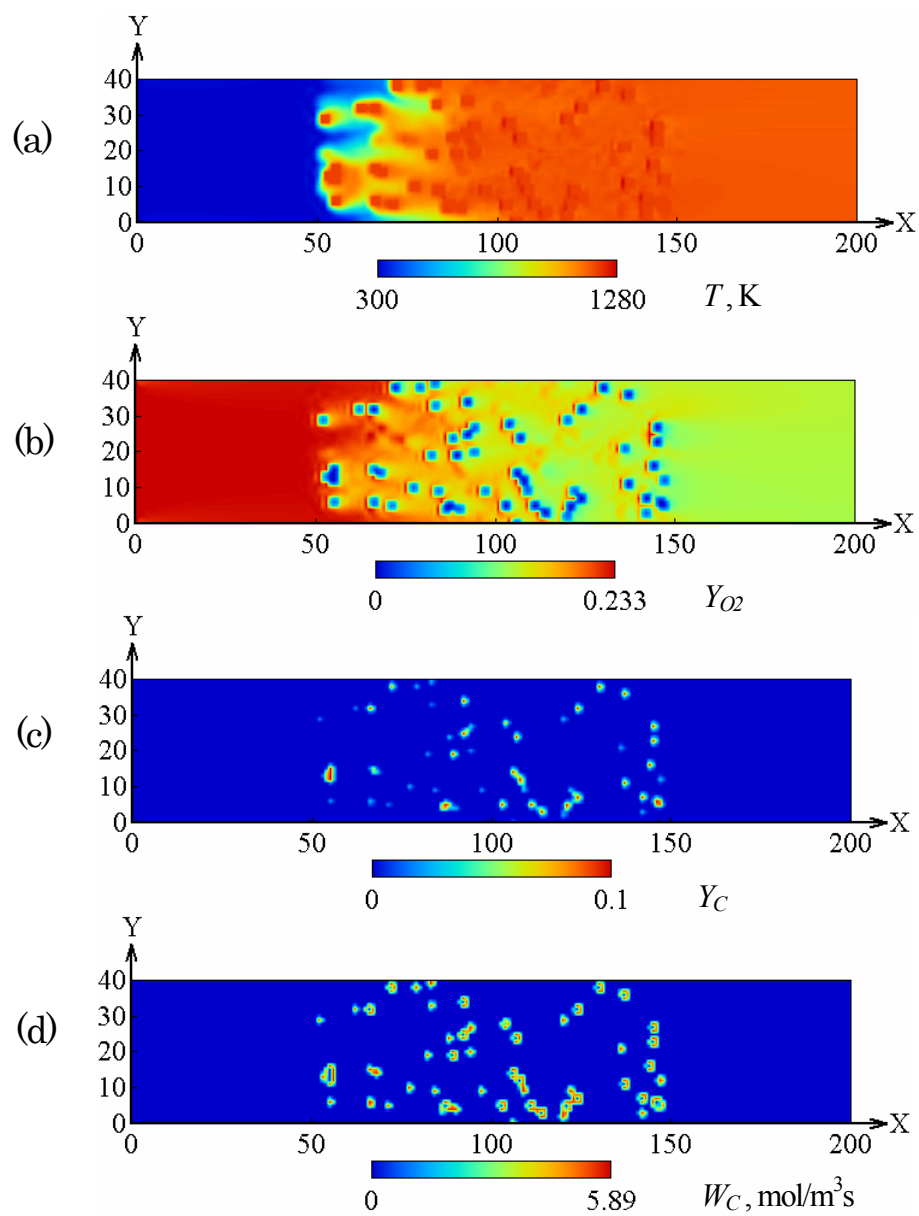


Figure 7 Distributions of (a) temperature, (b) oxygen, (c) soot, and (d) reaction rate. Each is cross sectional profile obtained in x - y plane at $D = 3$, $e = 0.9$, and $t = 0.63$ s.

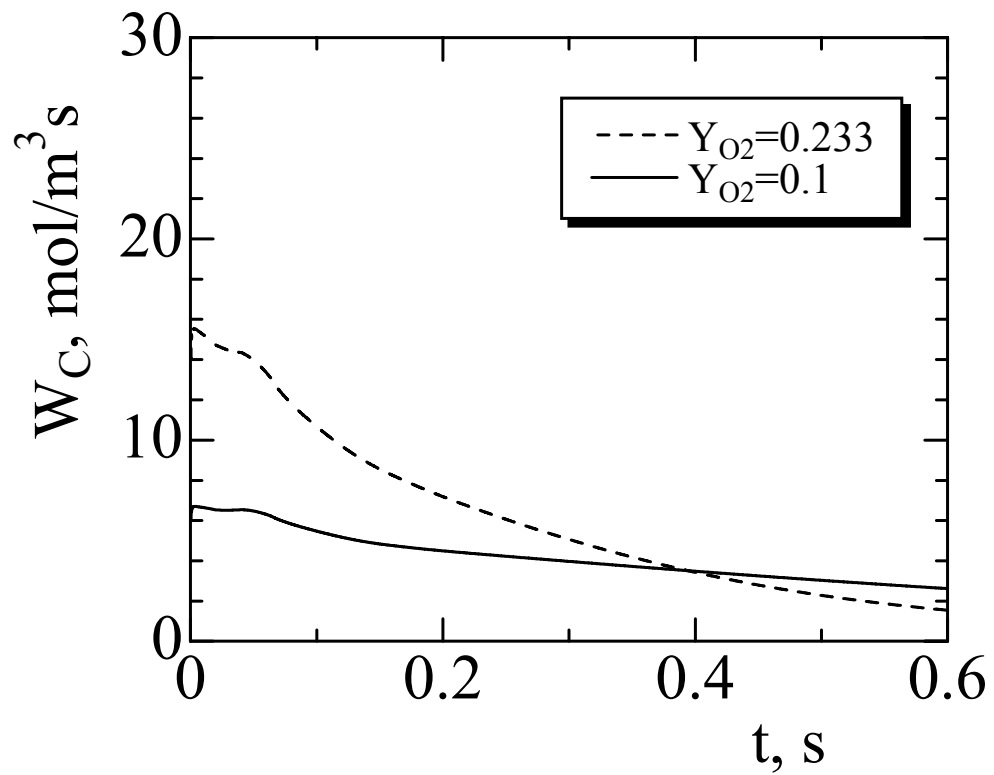
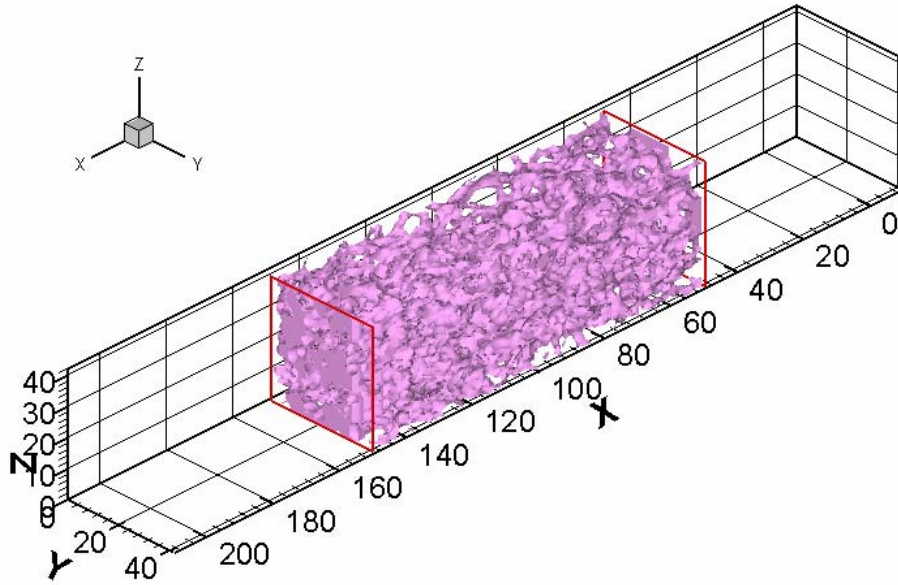
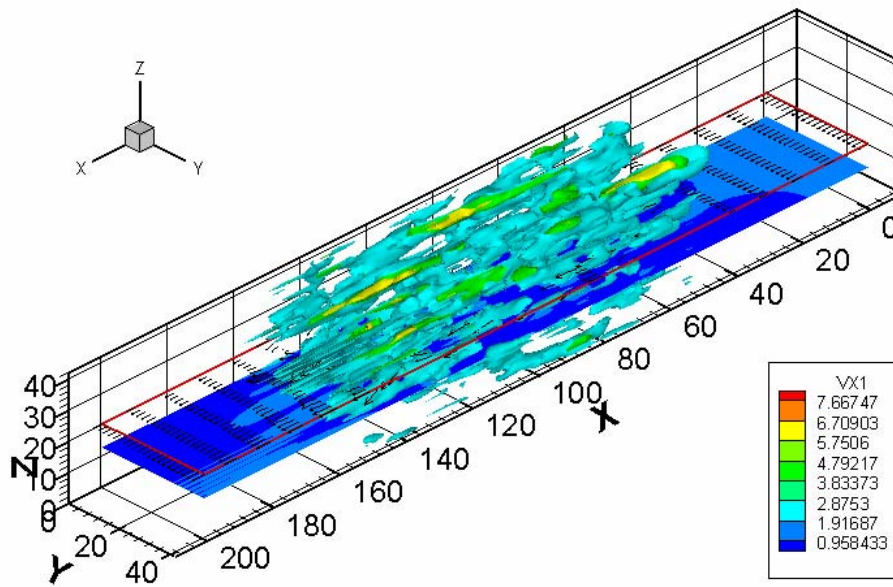


Figure 8 Mean reaction rate of soot as a function of time, with oxygen mass fraction of 0.1 and 0.233 in inflow.

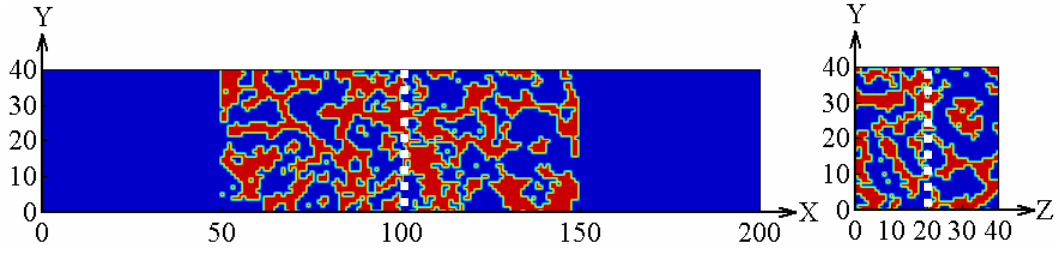


(a) Porous structure

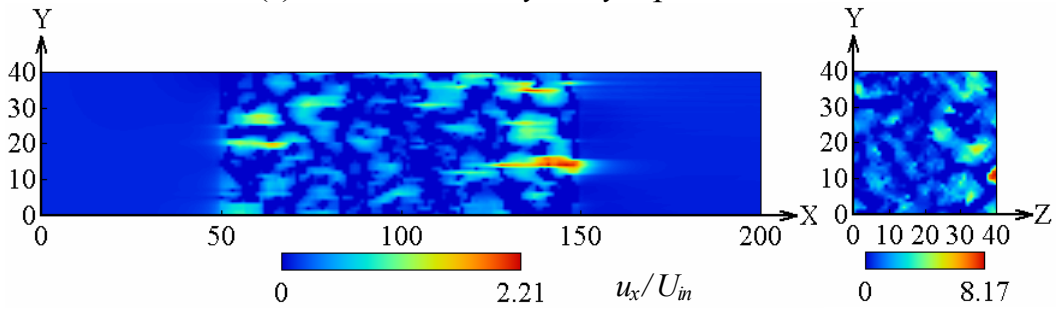


(b) Velocity of u_x/U_{in}

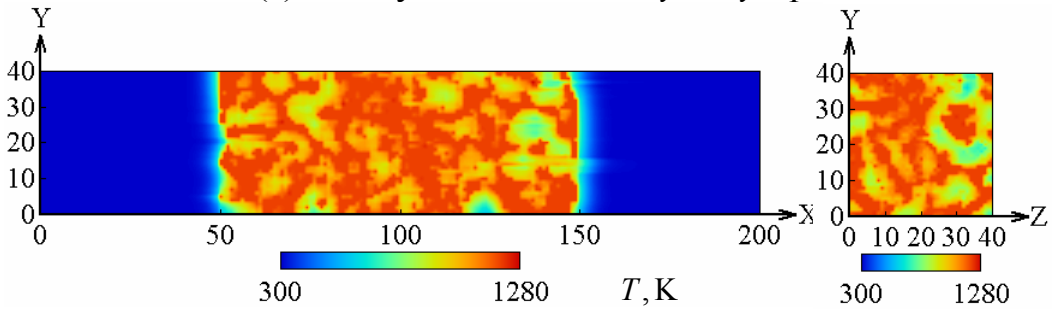
Figure 9 Three dimensional profiles of porous structure and non-dimensional velocity in x -direction. Ni-Cr metal is used for porous wall geometry. The local velocity is accelerated with soot combustion.



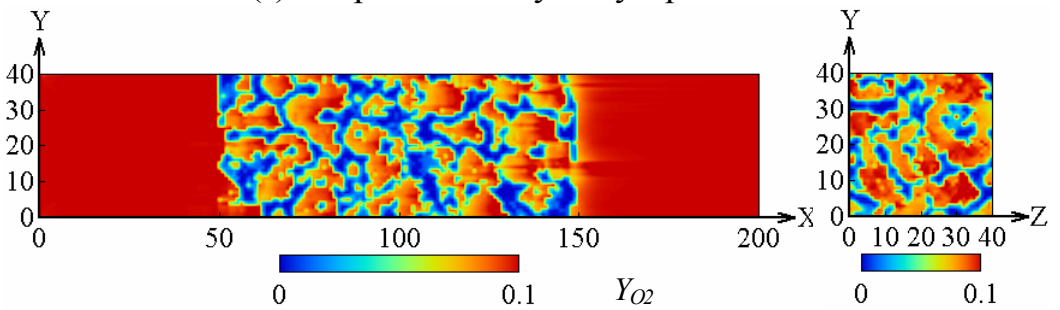
(a) Porous wall in x - y and y - z planes



(b) Velocity in x -direction at x - y and y - z planes



(c) Temperature in x - y and y - z planes



(d) Mass fraction of oxygen in x - y and y - z planes

Figure 10 Combustion field in porous media. Profiles in x - y and y - z planes are shown. Oxygen mass fraction in inflow is 0.1. Inhomogeneous combustion of soot is observed.